River flow forecasting using a rainfall disaggregation model incorporating small-scale topographic effects

R Misumi, V A Bell and R J Moore, *Centre for Ecology and Hydrology, Wallingford, Oxfordshire, OX10 8BB, UK*

River flow forecasting using rainfall predictions from a mesoscale weather prediction model in combination with a physically-based rainfall disaggregation model incorporating small-scale topographic variability is demonstrated. Rainfall predicted by the UK Met Office Mesoscale Model on a 16.8 km grid is disaggregated onto a 2 km grid using a rainfall model which adds the effect of small-scale topography. River flow is calculated by a distributed rainfall-runoff model using the output from the rainfall model. A thunderstorm event on 7 June 1996 over the Brue catchment in Somerset, England is used to evaluate the models. The rainfall model successfully forecasts the band-shaped rainfall field within the catchment and the error in the total amount of flow during the storm is only −12%. An error of −40% in the peak flow is attributed to the treatment of convective clouds in the model.

1. Introduction

River flow forecasting is very important as a basis for early flood warning. For forecasts more than 12 hours ahead, it is necessary to use rainfall data predicted by a mesoscale weather forecast model as the input to a rainfall-runoff model. However, because the grid size of operational mesoscale forecast models is still too coarse (16 km at best) to predict catchment-scale rainfall smaller than 200 km², this method has not been used except for a large-scale catchment (Miller & Kim, 1996). One way of constructing river flow forecasts using mesoscale model output is to disaggregate the rainfall data onto a smaller grid.

To disaggregate the rainfall data provided by a mesoscale model, a fine-mesh full-dynamic cloud model may be used (e.g. Lilly, 1990). However, such a model requires sophisticated initial conditions and a supercomputer for calculation, and thus does not present a realistic approach for operational use at present. Another approach to spatial rainfall disaggregation is to use a 'diagnostic' rainfall model capable of estimating small-scale precipitation using mesoscale meteorological data. The basic concept of such models is recalculation of the rainfall field by introducing the effect of small-scale topography which is not allowed for in the large-scale model. This type of model was first presented by Collier (1975). He demonstrated that the mean error of the simulated rainfall was 10% over an area of 1000 km² and 20% over 100 km². Bell (1978) improved this model by introducing cloud physics. Similar models have been developed by Alpert (1986) and Sinclair (1994).

The merit of a Collier-type model is simplicity. It requires only a workstation or a personal computer for calculation. On the other hand, the weakness of the model is its treatment of convection. It does not explicitly represent the behaviour of individual convective clouds. The precipitation from convective clouds is calculated by the cumulus parameterisation used in a large-scale model. However, it is known that the distribution of rainfall is strongly dependent on small-scale topography, especially for heavy rainfall events (e.g. Oki *et al.*, 1991); thus this type of model is considered to be useful for rainfall disaggregation for a storm event.

The validity of a Collier-type model and its possible value for hydrological use has been emphasised by many workers (Collier, 1975; Bell, 1978; Alpert & Shafir, 1989; Sinclair, 1994). However, there is no study that actually attempts river flow forecasting using such models. In the present study we carry out river flow forecasting using a rainfall model similar to that developed by Collier (1975). The rainfall data predicted by the UK Met Office Mesoscale Model, provided on a 16.8 km grid, are disaggregated onto a 2 km mesh. River flow is calculated by a grid-based distributed rainfall-runoff model developed by the Centre for Ecology and Hydrology (Moore & Bell, 1996; Bell & Moore, 1998a, 1998b). We investigate a case study of a thunderstorm event over the Brue catchment in southwest England using the models. The accuracy of river flow forecasting with this method is discussed.

2. Models

2.1. Outline of the procedure

Figure 1 shows the procedure adopted for river flow forecasting. The UK Met Office Mesoscale Model employs the Unified Model, which is non-hydrostatic and compressible, and whose spatial resolution is 0.15 degrees (16.8 km) in the horizontal with 28 levels in the vertical. An outline of the Unified Model is given by Cullen (1993). Mesoscale Model predictions of horizontal wind ($\bar{u}$, $\bar{v}$), pressure ($\bar{p}$), temperature ($\bar{T}$), relative humidity (r_h) and rainfall intensity at the surface ($\bar{I}$) are provided to the rainfall model every 15 minutes. The rainfall model disaggregates the rainfall data onto a 2 km grid which are then passed to the rainfall-runoff model configured on the same grid. A simple distributed rainfall-runoff model is used which employs a soil water accounting procedure within each 2 km grid square and an advection-diffusion routing model based on isochrone and storage concepts (Moore, Bell, Roberts et al., 1994; Moore & Bell, 1996; Bell & Moore, 1998a, 1998b). The basic formulation of the rainfall-runoff model is outlined in Appendix A. River flow is calculated by the model every 15 minutes.

2.2. Formulation of the rainfall model

The concept of the rainfall model used in this study is the same as that in Collier (1975), Bell (1978), Alpert (1986) and Sinclair (1994), which calculates the rainfall field by adding the effects of small-scale topography
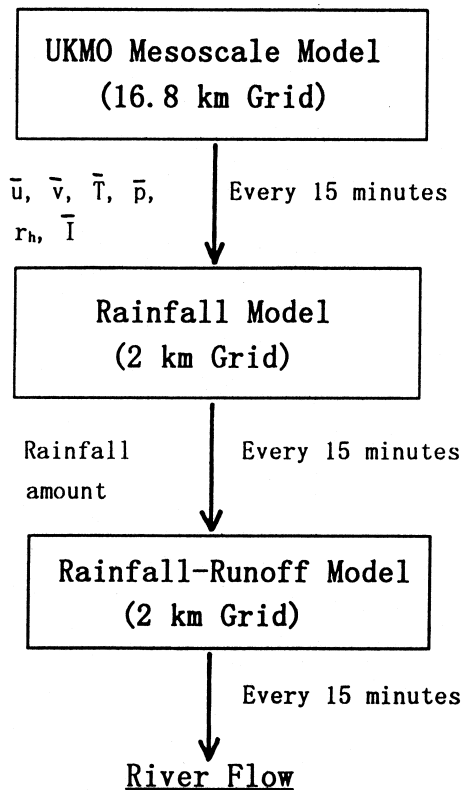

Figure 1. *Procedure for river flow forecasting.*

not treated in the Mesoscale Model. The modification here is the introduction of a terrain-following coordinate system to support the raindrop drift calculation. First of all, the continuity equation of the raindrop mixing ratio (the mass of raindrops per unit mass of dry air), Q_r, is given by (e.g. Kessler, 1969):

$$\frac{\partial Q_r}{\partial t} = -u\frac{\partial Q_r}{\partial x} - v\frac{\partial Q_r}{\partial y} - w\frac{\partial Q_r}{\partial z} + \frac{1}{\rho}\frac{\partial}{\partial z}\left(\rho V_r Q_r\right) + P_1 - E_1 \tag{1}$$

where x, y and z are the space coordinates increasing eastward, northward and upward respectively, t is time, u, v and w are the wind components, ρ is the density of air, V_r is the fall speed of raindrops, P_1 and E_1 are the production and evaporation rates of Q_r respectively. Physical quantities in equation (1) can be separated into mesoscale fields (denoted by overbars) and small-scale perturbations (denoted by primes) as:

$$\frac{\partial(\overline{Q_r}+Q_r')}{\partial t} = -\bar{u}\frac{\partial(\overline{Q_r}+Q_r')}{\partial x} - \bar{v}\frac{\partial(\overline{Q_r}+Q_r')}{\partial y} - \overline{w}\frac{\partial(\overline{Q_r}+Q_r')}{\partial z}$$
$$+ \frac{1}{\bar{\rho}}\frac{\partial}{\partial z}\left[\bar{\rho}V_r(\overline{Q_r}+Q_r')\right] + (\overline{P_1}+P_1') - (\overline{E_1}+E_1') \tag{2}$$

In equation (2) air density and wind components involved in advection are approximated by those in the mesoscale field. The terminal velocity of raindrops, V_r, is not separated because the raindrops produced by the mesoscale forcing and those formed by the small-scale perturbation are assumed to fall together with the same speed. Here $\overline{Q_r}$ satisfies the following equation:

$$\frac{\partial \overline{Q_r}}{\partial t} = -\bar{u}\frac{\partial \overline{Q_r}}{\partial x} - \bar{v}\frac{\partial \overline{Q_r}}{\partial y} - \overline{w}\frac{\partial \overline{Q_r}}{\partial z} + \frac{1}{\bar{\rho}}\frac{\partial}{\partial z}\left[\bar{\rho}V_r\overline{Q_r}\right] + \overline{P_1} - \overline{E_1}$$

Thus equation (2) is reduced to:

$$\frac{\partial Q_r'}{\partial t} = -\bar{u}\frac{\partial Q_r'}{\partial x} - \bar{v}\frac{\partial Q_r'}{\partial y} - \overline{w}\frac{\partial Q_r'}{\partial z} + \frac{1}{\bar{\rho}}\frac{\partial}{\partial z}\left[\bar{\rho}V_r Q_r'\right] + P_1' - E_1' \tag{3}$$

Assuming a steady state then:

$$0 = -\bar{u}\frac{\partial Q_r'}{\partial x} - \bar{v}\frac{\partial Q_r'}{\partial y} - \overline{w}\frac{\partial Q_r'}{\partial z} + \frac{1}{\bar{\rho}}\frac{\partial}{\partial z}\left[\bar{\rho}V_r Q_r'\right] + P_1' - E_1' \tag{4}$$

In the present model we consider the effects of small-scale topography as the perturbation. Thus Q_r' here represents the deviation of raindrop mixing ratio caused by additional condensation (P_1') and evaporation (E_1') due to small-scale topographic forcing. The steady-state assumption implies that the distribution of Q_r' instantaneously adjusts to the mesoscale field. Strictly speaking this is not correct. However, because the parameters given by the Mesoscale Model are not so exact as to calculate the rainfall variation within the time-step (15 minutes), this assumption is considered to be acceptable.

Because the values of $\bar{u}$, $\bar{v}$, $\overline{w}$ and $\bar{p}$ are directly provided from the Mesoscale Model, equation (4) can be solved for Q_r' numerically when V_r, $\overline{Q_r}$, P_1' and E_1' are parameterised. This equation is solved here on the ter-

rain-following coordinate system to support the rain-drop drift calculation. The coordinate transformation, parameterisations for V_r, $\overline{Q}_r$, P'_1 and E'_1, and numerical schemes are given in Appendix B. Finally, rainfall intensity, I, is calculated as:

$$I = V_r\left(\overline{Q}_r + Q'_r\right) \qquad (5)$$

The horizontal domain of the calculation is 40 km and 36 km in the x and the y direction, respectively. In order to avoid the underestimation of drifting rain-drops near the lateral boundaries, the region of 20 km by 16 km near the centre of the domain is used for the assessment (the region shown in Figure 2(b)). The horizontal grid size is 2 km in both directions. The top of the vertical domain is at the 10 km level, and the vertical layer is divided into 20. Variables in the Mesoscale Model are interpolated onto a 2 km grid using the multiquadric method (Moore, May, Jones et al., 1994) before they are passed to the rainfall model. The gradient of Q'_r is assumed to be zero at all the boundaries.

3. Case study

3.1. Description of the catchment

The Brue catchment in Somerset, England, is used in a case study to assess the approach. Figure 2 shows the location and the topography of the Brue catchment. The drainage area of the catchment is 135 km². It includes hills rising to about 150 m to the east, whilst the western part is relatively low-lying. This catchment has been the focus of the Hydrological Radar Experiment, HYREX (Moore, Carrington, Jones et al., 1994). The catchment is equipped with 49 recording raingauges and is continuously scanned by two operational radars to the west and south. The dense rain-gauge network provides the opportunity to evaluate the performance of the rainfall model with significant accuracy.

3.2. The event of 7 June 1996

On 7 June 1996 the weather in England was unstable. An episode of thundery rain was observed from morning to midnight. In the evening after 1800 GMT, strong thunderstorms passed over south England and rainfall in excess of 20 mm was observed around the Brue catchment. Figure 3 shows the sea-level pressure at 1800 GMT on 7 June 1996. There are two fronts across Britain with thunderstorms developing.

Figure 4(a) is the radar-echo pattern at 2000 GMT derived from the Wardon Hill radar located 40 km south of the Brue catchment. A cluster of radar echoes passed through southern England, with the direction of storm movement from south-southwest to north-northeast. The development and movement of the cluster are successfully forecast by the Mesoscale Model (Figure 4(b)). However, the cluster consists of one large and weak cell in the model forecast, while it is actually composed of several small and strong cells as indicated by the radar observation. In addition, the cluster has already passed the Brue catchment in the Mesoscale Model forecast, while it is still over the catchment as indicated by the radar observation.

For the evaluation of model performance, the following three measures are used: the root mean square error (rmse), the correlation coefficient (r_c) and the goodness of fit (R^2). The definitions of the measures are given in Appendix C.

The initial condition of the Mesoscale Model forecast is the analysis at 1200 GMT on 7 June 1996. Rainfall forecasts are made every 15 minutes until 2200 GMT on 8 June 1996. River flow forecasts are constructed using rainfall model output for the 48-hour period starting at 1200 GMT on 7 June 1996. The parameters used in the rainfall-runoff model have been calibrated using the observed flow from 0000 GMT on 1 April to 0000
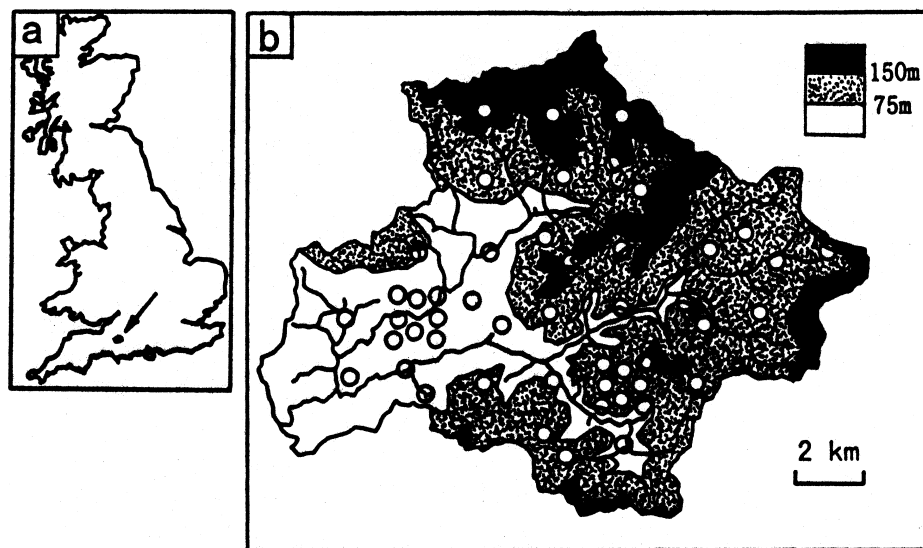

Figure 2. (a) The location of the Brue catchment within the UK. (b) Topography and raingauge network within the Brue catchment. (Hatched area: higher than 75 m; black area: higher than 150 m; the open circles denote raingauges.)
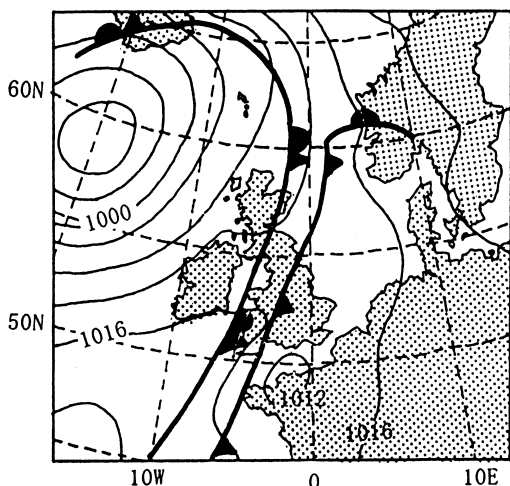
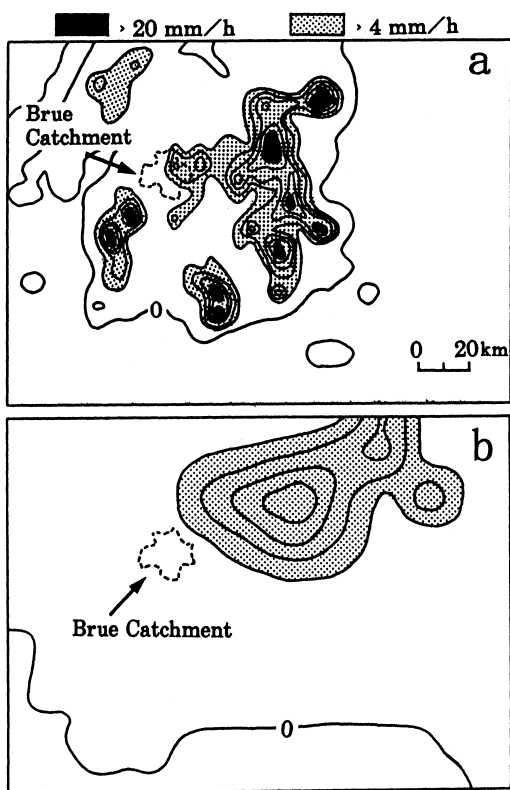**Figure 3.** *Surface sea-level pressure at 1800 GMT on 7 June 1996. Contours are drawn every 4 hPa.*

Figure 4. *Rainfall intensity at 2000 GMT on 7 June 1996 (a) derived from Wardon Hill C-band radar and (b) forecast by the Mesoscale Model. Contours are drawn every 4 mm h⁻¹.*

Figure 5. *Distribution of total rainfall from 1200 GMT to 2200 GMT on 7 June 1996 using raingauges, the Mesoscale Model and the rainfall model.*

GMT on 7 June 1996. In order to minimise the effect of initial conditions, the rainfall-runoff model had been run for one month using raingauge data before being used for forecasting.

3.3. Forecast result

Figure 5 compares the horizontal distribution of total rainfall from 1200 GMT to 2200 GMT on 7 June. The raingauge observations indicate that the rainfall is distributed in a band running from south-southwest to
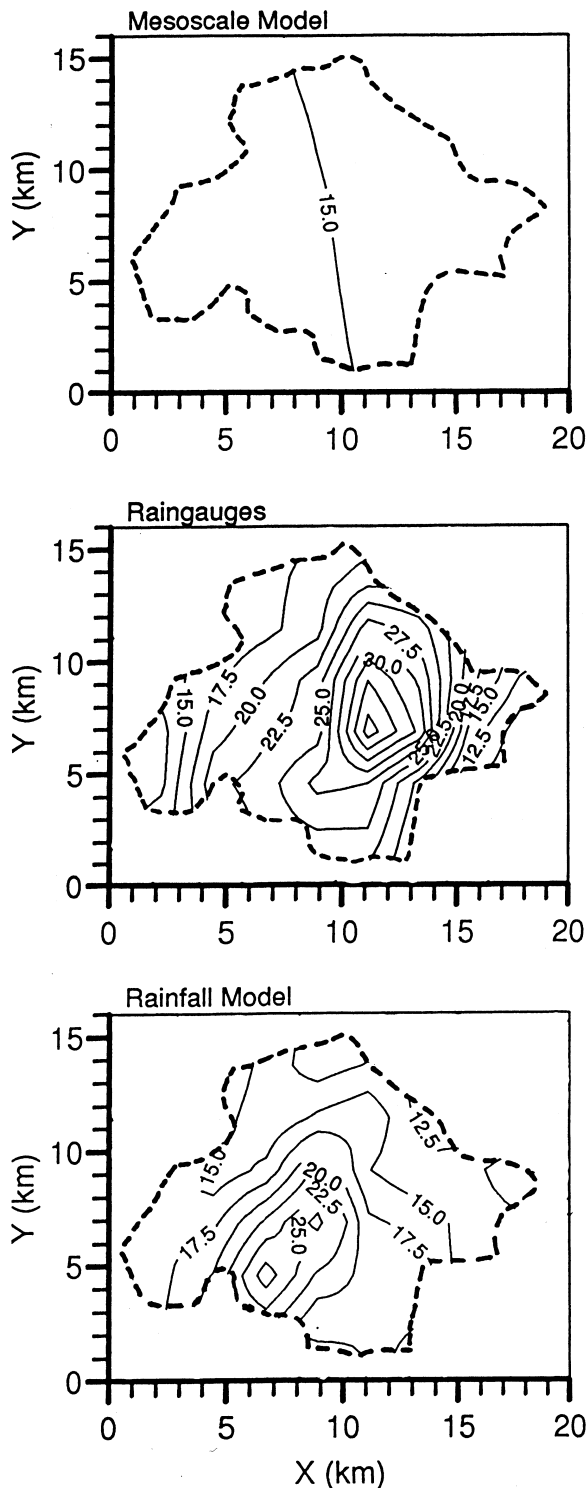
north-northeast with the maximum rainfall reaching 37.5 mm. By comparison, the rainfall is distributed almost uniformly in the Mesoscale Model. This is because the grid size of the Mesoscale Model is too coarse to predict the rainfall distribution within the catchment. However, the band-shaped rainfall pattern is predicted by the rainfall model although the band is located slightly to the west of that observed. The max-

imum rainfall from the rainfall model is 27.5 mm, which is 26.7% smaller than the observed amount.

Figure 6 compares the time variation of the hourly catchment average rainfall based on the raingauges, the Mesoscale Model and the rainfall model. The raingauge data are interpolated onto the 2 km grid using the multi-quadric method and the catchment average rainfall obtained as the area-weighted mean rainfall of all the grid rainfalls. A strong peak in rainfall which reaches 9 mm h^{-1} is observed by the raingauges at 2100 GMT. The existence of the peak is forecast by the Mesoscale Model, but its intensity is much weaker and it appears an hour earlier than the raingauge observation. This is consistent with Figure 4 which shows that the cluster of strong echoes is forecast as a weak rainfall region which has passed over the Brue catchment earlier than that observed. With the use of the rainfall model, the underestimation of the rainfall peak is slightly corrected. It should be noted that the rainfall from the rainfall model indicates larger values especially when heavy rainfall is predicted. This reflects the fact that the low-level air is moist and favourable for orographic enhancement when rainfall is strong. However, the peak in the model rainfall is still weaker and the timing is earlier than that indicated by the raingauge data.

The model performance in terms of catchment average rainfall and rainfall distributions is summarised in Table 1. The error in the total rainfall amount is –29% for the Mesoscale Model. This underestimation is corrected by the rainfall model, reducing the error to –19.7%. The error in the maximum hourly rainfall is also reduced from –36.7% to –28.9%. R^2 and the *rmse* statistics for the time variation of catchment-average rainfall are slightly improved by the rainfall model. A negative correlation coefficient is obtained for the rainfall distribution of the Mesoscale Model, but this becomes positive for the rainfall model with a value of 0.21. The *rmse* for the distribution of the total rainfall, which is relative to the interpolated raingauge data on the 32 grid points in the catchment, reduces by 1.1 mm (5%) with the use of the rainfall model.
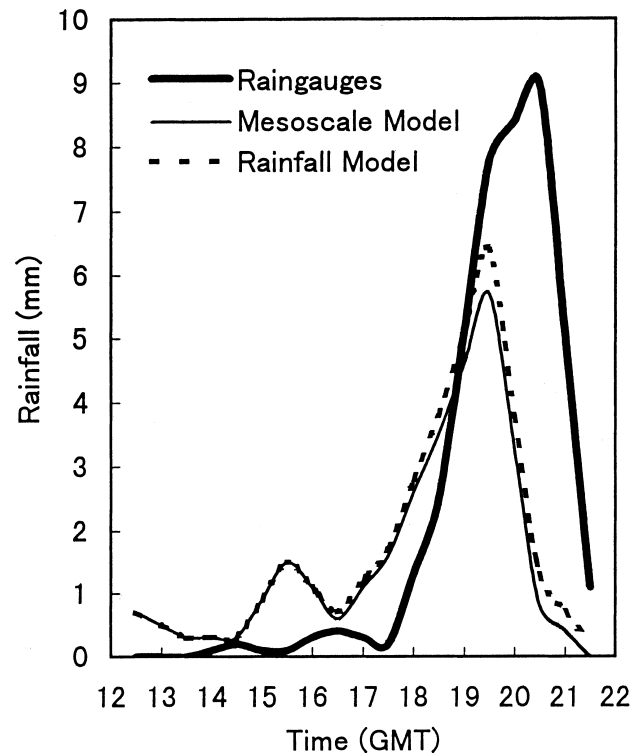

Figure 6. *Time variation of hourly catchment-average rainfall using raingauge data and forecasts from the Mesoscale Model and the rainfall model for the period 1200 UTC on 7 June to 1200 UTC on 9 June 1996.*

Figure 7 shows the observed and rainfall-runoff model predicted hydrographs for the 48-hour period starting 1200 GMT on 7 June. The forecast hydrograph obtained using raingauge data is slightly different from the observed flow. This is due in part to the calibration error of the rainfall-runoff model. The hydrographs produced using Mesoscale Model and rainfall model outputs begin to rise earlier than the observed flow, reflecting the overestimation of rainfall before 1800 GMT (Figure 6). However, the time of the peak flow is nearer to that observed than when raingauge data are used. This is because the model calibration error offsets the error of the rainfall prediction. Performance measures for flow forecasts are shown in Table 2. The error

Table 1. *Performance measures for catchment-average rainfall and for the distribution of total rainfall from 1200 GMT to 2200 GMT on 7 June 1996. The rmse and R^2 statistics for the catchment-average rainfall are calculated over 41 data values in the period. The rmse and r$_c$ statistics for the rainfall distribution are computed over 32 grid-points within the catchment.*

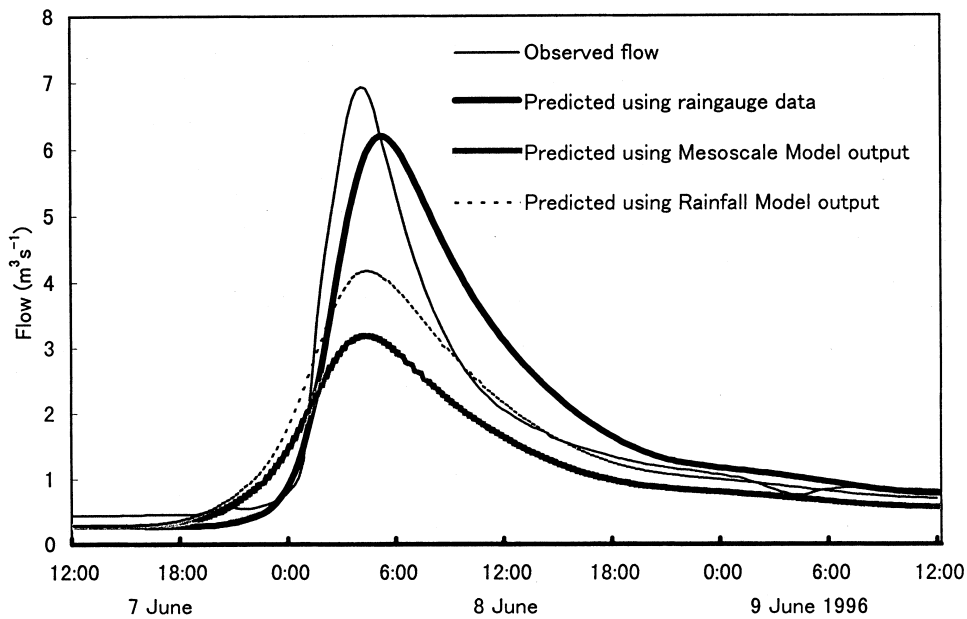| Data type	Catchment-average rainfall				Rainfall distribution	
	Total amount (Error)	Hourly maximum (Error)	R^2	rmse	r$_c$	rmse
Raingauge	21.3 mm	9.0 mm	–	–	–	–
Mesoscale Model	15.1 mm (–29.0%)	5.7 mm (–36.7%)	0.32	4.1 mm	–0.39	9.7 mm
Rainfall model	17.1 mm (–19.7%)	6.4 mm (–28.9%)	0.35	4.0 mm	0.21	8.6 mm

301

Figure 7. *Hydrographs of observed flow and those forecast using raingauge data, the Mesoscale Model output and the rainfall model output for 7 June 1996.*

Table 2. *Comparison of the river flow from 1200 GMT on 7 June to 1200 GMT on 9 June. The rmse and R^2 are calculated over 193 data values in this period.*

Data types	Total amount of flow (Error)	Peak flow (Error)	R^2	rmse
Observation	$2.93 \times 10^5\,m^3$	$6.94\,m^3\,s^{-1}$	–	–
Predicted using raingauges	$3.20 \times 10^5\,m^3$ (9.1%)	$6.20\,m^3\,s^{-1}$ (−10.6%)	0.87	$1.34\,m^3\,s^{-1}$
Predicted using Mesoscale Model	$2.03 \times 10^5\,m^3$ (−30.8%)	$3.19\,m^3\,s^{-1}$ (−54.0%)	0.63	$2.24\,m^3\,s^{-1}$
Predicted using rainfall model	$2.58 \times 10^5\,m^3$ (−11.9%)	$4.18\,m^3\,s^{-1}$ (−39.8%)	0.81	$1.54\,m^3\,s^{-1}$

in the total amount of flow is −30.8% for the Mesoscale Model prediction. With the use of the rainfall model, the error decreases to −11.9%. The peak flow error is −10.6% when raingauge data are used, −54.0% using the Mesoscale Model data and −39.8% using the rainfall model data. The error in the rainfall model prediction is attributed to the underestimation of the maximum rainfall intensity (Figure 6). The goodness of fit, R^2, is considerably improved by the rainfall model, which reflects the small error in forecasting the total flow amount.

4. Summary and discussion

River flow forecasts were produced for the thunderstorm event on 7 June 1996 over the Brue catchment in southeast England. The rainfall forecasts from the UK Met Office Mesoscale Model, provided on a 16.8 km grid, were disaggregated onto a 2 km grid using a rainfall model which adds the effect of finer-scale topography to the Mesoscale Model output. River flow was forecast using a distributed rainfall-runoff model con-

figured on the same 2 km grid. The results obtained indicate that the error in the predicted total amount of flow is −11.9%, while that of the peak flow is −39.8%.

The rainfall model has the effect of reducing the error in the maximum rainfall intensity from the Mesoscale Model (Figure 6). It strengthens the rainfall especially when heavy rainfall is predicted, because the low-level air is moist and favourable for orographic enhancement during the strong rainfall period. However, the maximum rainfall intensity from the rainfall model is still smaller than that from the raingauges. As shown in Figure 4, the Mesoscale Model forecasts a cluster of convective cells as a broad and weak rainfall region. It is considered that not only the effect of small-scale topography but also the behaviour of such convective cells contributed to the strong peak. Introduction of the behaviour of the convective cells into the rainfall model is necessary for further reduction of the error.

The rainfall model successfully forecasts the band-shaped rainfall region within the catchment, although the predicted band was located slightly to the west of

that observed (Figure 5). In addition, the correlation coefficient relative to the observed rainfall pattern changes from negative to positive under the influence of the rainfall model (Table 1). This fact suggests that the rainfall model is a useful tool in estimating the rainfall pattern within the catchment. The slight difference in the location of the band is considered to be caused by the effect of convective cells; probably, the eastern side of the band, which is not predicted by the rainfall model, was produced by the passage of convective cells.

The total amount of flow is well forecast by the models (Table 2). This is due to the total amount of rainfall during the storm also being predicted well (Table 1). The result is not unexpected because other workers also show good results for the simulation of 3-hour to 24-hour total rainfall using similar models (Collier, 1975; Bell, 1978; Alpert & Shafir, 1989; Sinclair, 1994). The good result in this case is due to the fact that the errors in the rainfall peak are offset by the overestimation of the rainfall before 1800 GMT (Figure 5). More case studies are needed to support this result. On the other hand, the error in the peak flow is relatively large. This is apparently due to the underestimation of the maximum rainfall intensity. As discussed above, it is considered that the behaviour of convective cells is the main cause for this error.

This study is the first demonstration of river flow forecasting for a small catchment using mesoscale model output. The result here is for a moderately hilly catchment. It is likely that the rainfall model will be of even greater use for mountainous catchments where strong orographic rainfall is experienced. Results from further case studies are needed to clarify whether or not this approach is useful for early flood warning.

Appendix A. Formulation of the rainfall-runoff model

The rainfall-runoff model used in this study is of a distributed type which employs a simple soil water accounting procedure within each 2 km grid square and an advection-diffusion routing model based on isochrone and storage concepts. Generation of runoff from a given grid-square is accomplished by conceptualising the grid-square as a simple storage. The key element in the conceptualisation is that the depth of the store representing water absorption capacity is determined by the average terrain gradient within the square as measured from a digital terrain model (DTM). Specifically, the following linkage function is used to relate maximum storage capacity, S_{max}, to the average terrain gradient, $\bar{a}$, within a grid-square:

$$S_{max} = \left(1 - \frac{\bar{a}}{a_{max}}\right) c_{max}$$

The parameters a_{max} and c_{max} are upper limits of gradient and storage capacity respectively and act as 'regional parameters' for the catchment. A measurement of average terrain gradient for each grid square of the catchment is obtained from the DTM.

A grid storage loses water in three possible ways. If the storage is fully saturated from previous rainfall then any net addition of water spills over and contributes 'direct runoff' to the fast catchment response. Drainage from the base of the store is controlled by the volume of water in store and contributes to the slow catchment response. Thirdly, water is lost via evaporation to the atmosphere. Specifically, a water balance is maintained as follows for each grid square and time interval of duration Δt. Evaporation loss occurs at the rate, E_a, which is related to the potential evaporation rate, E, through the relation:

$$E_a = \begin{cases} \left(1 - \dfrac{D - D^*}{S_{max} - D^*}\right) E & D \le D^* \\ E & D > D^* \end{cases}$$

where $D = S_{max} - S$ is the storage deficit and D^* is the threshold deficit below which evaporation occurs at the potential rate. The value of D^* is common across grid squares.

Drainage from the grid storage, which contributes to the slow catchment response, occurs at the rate:

$$d = \begin{cases} k_d S^\beta & S > 0 \\ 0 & \text{otherwise} \end{cases}$$

where k_d is the storage constant and the exponent β is a parameter (set here to 3).

The direct runoff rate is calculated as:

$$q = \max(0, S - S_{max}) + I \, \Delta t$$

where I is the rainfall rate and the updated water storage is given by:

$$S = \max(0, S + I \, \Delta t - E_a \, \Delta t - d \, \Delta t)$$

The construction of isochrones – lines joining points of equal time of travel to the basin outlet – has been achieved by assuming that water travels with only two velocities depending on whether it is associated with a hillslope or in a river channel. Each isochrone strip is represented by a discrete kinematic wave to introduce diffusion into the isochrone formulation. Specifically, the n isochrone strips are replaced by a cascade of n reaches, with the outflow from the kth reach at time t represented by:

$$q_t^k = (1 - \theta) q_{t-1}^k + \theta (q_{t-1}^{k+1} + r_t^k)$$

303

Here, r_t^k is the outflow rate from the kth isochrone strip calculated for the interval (t-1, t) and serves as the lateral inflow to the kth reach. The flow rate q_t^1 corresponds to the total outflow from the catchment. The parameter θ is related to the kinematic wave speed.

In the present context r_t^k relates to direct runoff or drainage depending on whether the routing model is used to represent the fast or slow pathway to the catchment outlet. The approach adopted here routes direct runoff and drainage separately using two parallel kinematic wave models, characterised by different wave speeds θ_s and θ_b respectively, but sharing the same spatial discretisation defined by the set of isochrones. The routing parameters θ_s and θ_b and drainage parameter k_d are estimated by calibration to give the best model fit.

Appendix B. The terrain-following coordinate and parameterisations

Equation (4) is transformed into the terrain-following coordinate system as follows. The vertical coordinate, ζ, is defined as:

$$\zeta = \frac{Z_t(z - Z_s)}{Z_t - Z_s}$$

where $Z_s(x, y)$ is the elevation at the ground and Z_t is the depth of the model domain. Equation (4) can be rewritten in the (x, y, ζ) system as:

$$0 = -\overline{u}\frac{\partial Q_r'}{\partial x} - \overline{v}\frac{\partial Q_r'}{\partial y} - \left(G_1\overline{u} + G_2\overline{v} + H\overline{w}\right)\frac{\partial Q_r'}{\partial \zeta} + \frac{H}{\overline{\rho}}\frac{\partial}{\partial \zeta}$$
$$[\overline{\rho}V_r Q_r'] + P_1' - E_1' \tag{B1}$$

where:

$$G_1 = \frac{\partial \zeta}{\partial x} = \frac{\zeta - Z_t}{Z_t - Z_s}\frac{\partial Z_s}{\partial x}$$

$$G_2 = \frac{\partial \zeta}{\partial y} = \frac{\zeta - Z_t}{Z_t - Z_s}\frac{\partial Z_s}{\partial y}$$

$$H = \frac{\partial \zeta}{\partial z} = \frac{Z_t}{Z_t - Z_s}$$

The transformation rate between water vapour and raindrops due to the topographic effect, P_c, following Sinclair (1994), is given by:

$$P_c = \lambda_1 \frac{Q_s \overline{T}}{\overline{p}}\left(\frac{LR - c_p R_v \overline{T}}{c_p R_v \overline{T}^2 + Q_s L^2}\right)\overline{\rho}gw'$$

where Q_s is the saturation mixing ratio of water vapour, L is the latent heat of condensation, R is the gas constant for dry air, R_v is the gas contant for water vapour, c_p is the specific heat at constant pressure, g is the acceleration due to gravity, w' is the vertical velocity due to small scale topography, and:

$$\lambda_1 = \begin{cases} \left(\dfrac{r_h - 0.6}{0.4}\right)^{0.5} & r_h > 0.6 \\ 0 & \text{otherwise} \end{cases}$$

The parameter λ_1 represents the dependence of P_c on the relative humidity (r_h). It is assumed that condensation occurs when $w' > 0$ and raindrops evaporate when w' is negative. Thus:

$$P_1' = \begin{cases} P_c & w' > 0 \\ 0 & \text{otherwise} \end{cases}$$

and

$$E_1' = \begin{cases} P_c & w' > 0 \text{ and } Q_r + Q_r' > 0 \\ 0 & \text{otherwise} \end{cases}$$

If it is assumed that an orographic updraught is proportional to the inner product between the horizontal wind vector ($\mathbf{V}_s$) and the gradient of topography (∇Z_s), w' can be written as the difference between the updraught due to the 'real' topography and that due to the Mesoscale Model topography. Thus:

$$w' = \lambda_2(\mathbf{V}_s \cdot \nabla Z_s - \mathbf{V}_s \cdot \nabla Z_m)$$

where Z_s is the height of topography for the rainfall model and Z_m is that for the Mesoscale Model. In the present study the geopotential height at the ground level of the Mesoscale Model is used for Z_m. The parameter λ_2 defines the vertical profile of the orographic updraught, given by Sinclair (1994) as:

$$\lambda_2 = \begin{cases} \left(\dfrac{p - p_t}{p_s - p_t}\right)^{\tan\left(\frac{\gamma\pi}{4}\right)} & p < p_t \\ 0 & \text{otherwise} \end{cases}$$

where p_s is the pressure at the ground, $p_t = 200$ hPa and $\gamma = 0.7$.

For the fall speed of raindrops, the formulation of Ogura & Takahashi (1971) is used:

$$V_r = 31.2[\overline{\rho}(\overline{Q}_r + Q_r')]^{0.125} \tag{B2}$$

The raindrop mixing ratio in the Mesoscale Model, $\overline{Q}_r$, is related to the rainfall intensity in the Mesoscale Model, $\overline{I}$, by:

$$\overline{I} = V_r \overline{Q}_r \tag{B3}$$

Here $\overline{I}$ is assumed to be constant in the vertical direction. Equations (B1), (B2) and (B3) are solved by an iteration method. Specifically equation (B1) is replaced by a finite-difference equation and integrated in time until the left hand side ($\partial Q_r'/\partial t$) becomes zero. At every step of this integration, the values of Q_r and V_r are estimated from equations (B2) and (B3) by the Newton-Raphson method. A forward scheme in time

and an upstream scheme in space are used for the integration.

Appendix C. Definition of performance measures

The definition of *rmse* is:

$$rmse = \left[\frac{1}{N} \sum (Q_n - q_n)^2 \right]^{0.5}$$

where Q_n and q_n are the observed and forecast value at the time n or the point n. The summation is computed over N values in space or time.

The correlation coefficient, r_c, is defined as:

$$r_c = \frac{\sum (Q_n - \overline{Q})(q_n - \overline{q})}{[\Sigma(Q_n - \overline{Q})^2]^{0.5} [\Sigma(q_n - \overline{q})^2]^{0.5}}$$

where $\overline{Q}$ and $\overline{q}$ are the mean of the observations and forecasts, respectively, over the N points. Criterion r_c is only used for evaluation of the rainfall distribution.

The goodness of fit, R^2, is defined as:

$$R^2 = 1 - \frac{\Sigma(Q_n - q_n)^2}{\Sigma(Q_n - \overline{Q})^2}$$

This can be interpreted as the proportion of variance in the observations accounted for by the model forecasts. This criterion is used for the evaluation of the forecast hyetograph and hydrograph.

References

Alpert, P. (1986). Mesoscale indexing of the distribution of orographic precipitation over high mountains. *J. Climate Appl. Meteorol.*, **25**: 532–545.

Alpert, P. & Shafir, H. (1989). Mesoγ-scale distribution of orographic precipitation: Numerical study and comparison with precipitation derived from radar measurement. *J. Appl. Meteorol.*, **28**: 1105–1117.

Bell, R. S. (1978). The forecasting of orographically enhanced rainfall accumulations using 10-level model data. *Meteorol. Mag.*, **107**: 113–124.

Bell, V. A. & Moore, R. J. (1998a). A grid-based distributed flood forecasting model for use with weather radar data. 1. Formulation. *Hydrology and Earth System Sciences*, **2**: 265–281.

Bell, V. A. & Moore, R. J. (1998b). A grid-based distributed flood forecasting model for use with weather radar data. 2. Case studies. *Hydrology and Earth System Sciences*, **2**: 283–298.

Collier, C. G. (1975). A representation of the effects of topography on surface rainfall within moving baroclinic disturbances. *Q. J. R. Meteorol. Soc.*, **101**: 407–422.

Cullen, M. J. P. (1993). The unified forecast/climate model. *Meteorol. Mag.*, **122**: 81–94.

Kessler, E. (1969). On the distribution and continuity of water substance in atmospheric circulations. *Meteorol. Monographs, No.10*, Am. Meteorol. Soc., 84 pp.

Lilly, D. K. (1990). Numerical prediction of thunderstorms – has its time come? *Q. J. R. Meteorol. Soc.*, **116**: 779–798.

Miller, N. L. & Kim, J. (1996). Numerical prediction of precipitation and river flow over the Russian river watershed during the January 1995 California storms. *Bull. Am. Meteorol. Soc.*, **77**: 101–105.

Moore, R. J. & Bell, V. A. (1996). A grid-based flood forecasting model using weather radar, digital terrain and Landsat data. *Quaderni Di Idronomia Montana*, **16**: 97–105.

Moore, R. J., Bell, V. A., Roberts, G. A. & Morris, D. G. (1994). Development of distributed flood forecasting models using weather radar and digital terrain data. *R&D Note 252, Research Contractor: Institute of Hydrology*, National Rivers Authority, 144 pp.

Moore, R. J., Carrington, D. S., Jones, D. A., Stewart, E. J., Hatton, R. & Aucott, L. (1994). The UK HYREX project. *Ann. Geophysicae*, **12**: Suppl. II, C402.

Moore, R. J., May, B. C., Jones, D. A. & Black, K. B. (1994). Local calibration of weather radar over London. In M. E. Almeida-Teixeira, R. Fantechni, R. Moore & V. M. Silva (eds.) *Advances in Radar Hydrology*, European Commission Report EHR 14334 EN, 186–195.

Ogura, Y. & Takahashi, T. (1971). Numerical simulation of the life cycle of a thunderstorm. *Mon. Wea. Rev.*, **99**: 895–911.

Oki, T., Musiake, K. & Koike, T. (1991). Spatial rainfall distribution at a storm event in mountainous regions, estimated by orography and wind direction. *Water Resour. Res.*, **27**: 359–369.

Sinclair, M. R. (1994). A diagnostic model for estimating orographic precipitation. *J. Appl. Meteorol.*, **33**: 1163–1175.